ELSEVIER

Chemical Engineering Science 61 (2006) 268–281

Chemical Engineering Science

www.elsevier.com/locate/ces

Predictive control of particle size distribution in particulate processes

Dan Shi, Nael H. El-Farra, Mingheng Li, Prashant Mhaskar, Panagiotis D. Christofides*

Department of Chemical Engineering, University of California, 405 Hilgard Avenue, Box 951592, Los Angeles, CA 90095-1592, USA

Received 1 June 2004; accepted 1 December 2004
Available online 27 June 2005

Abstract

In this work, we focus on the development and application of predictive-based strategies for control of particle size distribution (PSD) in continuous and batch particulate processes described by population balance models (PBMs). The control algorithms are designed on the basis of reduced-order models, utilize measurements of principle moments of the PSD, and are tailored to address different control objectives for the continuous and batch processes. For continuous particulate processes, we develop a hybrid predictive control strategy to stabilize a continuous crystallizer at an open-loop unstable steady-state. The hybrid predictive control strategy employs logic-based switching between model predictive control (MPC) and a fall-back bounded controller with a well-defined stability region. The strategy is shown to provide a safety net for the implementation of MPC algorithms with guaranteed stability closed-loop region. For batch particulate processes, the control objective is to achieve a final PSD with desired characteristics subject to both manipulated input and product quality constraints. An optimization-based predictive control strategy that incorporates these constraints explicitly in the controller design is formulated and applied to a seeded batch crystallizer. The strategy is shown to be able to reduce the total volume of the fines by 13.4% compared to a linear cooling strategy, and is shown to be robust with respect to modeling errors.

Keywords: Crystallization process; Population balance model; Model reduction; Model predictive control; Input constraints; Lyapunov-based bounded control

1. Introduction

Particulate processes are prevalent in a number of process industries including agricultural, chemical, food, minerals, and pharmaceuticals. By some estimates, 60% of the products in the chemical industry are manufactured as particulates with an additional 20% using powders as ingredients. Examples of particulate processes include the crystallization of proteins for pharmaceutical applications, the emulsion polymerization reactors for the production of latex, and the titania powder aerosol reactors used in the production of white pigments. One of the key attributes of particulate systems is the co-presence of a continuous phase and a dispersed phase, which leads to the occurrence of physico-chemical phenomena such as particle nucleation, growth, coagulation, and breakage which are absent in homogeneous processes and lead to a distributed characterization of the physical and chemical properties of the particulate product such as particle size, shape, morphology, porosity and molecular weight.

It is now well understood that the physico-chemical and mechanical properties of materials made with particulates are strongly dependent on the characteristics of the corresponding particle size distribution (PSD). For example, a nearly mono-disperse PSD is required for titania pigments to obtain the maximum hiding power per unit mass. Also, in coatings, the product's composition, molecular weight and PSDs often need to be maintained in specific ranges to ensure the coating has a desired level of film formation, film strength, and gloss. In all of these instances, the PSD provides the critical link between the product quality indices and the operating process variables; and, therefore, the ability to effectively manipulate the PSD is essential for our ability to control the end product quality in these processes. In this light, the problem of synthesizing and implementing

* Corresponding author. Tel.: +1 310 794 1015; fax: +1 310 206 4107.
E-mail address: pdc@seas.ucla.edu (P.D. Christofides).

0009-2509/$ - see front matter © 2005 Elsevier Ltd. All rights reserved.
doi:10.1016/j.ces.2004.12.059

high-performance model-based feedback control systems on particulate processes to achieve PSDs with desired characteristics has significant industrial value.

The mathematical models of particulate processes are typically obtained through the application of population, material and energy balances and consist of systems of nonlinear partial integro-differential equations that describe the evolution of the PSD, coupled with systems of nonlinear ordinary differential equations (ODEs) that describe the evolution of the state variables of the continuous phase. There is an extensive literature on population balance modeling, numerical solution, and dynamical analysis of particulate processes, see, for example, Pladis and Kiparissides (1998), Mantzaris et al. (2001), Friedlander (1977), Gelbard and Seinfeld (1978), Ramkrishna (1985), Hounslow (1990), Kumar and Ramkrishna (1996), Jerauld et al. (1983), Rawlings and Ray (1987), Randolph and Larson (1988); see also Christofides (2002) for further details and references. Early work on control of particulate processes focused mainly on the understanding of fundamental control-theoretic properties of PBMs (e.g., Semino and Ray, 1995a), and the application of conventional control schemes to crystallizers and emulsion polymerization processes (e.g., Semino and Ray, 1995b; Rohani and Bourne, 1990; Dimitratos et al., 1994 and the references therein). More recently, the realization that PBMs—owing to their infinite-dimensional nature—cannot be used directly for the synthesis of practically implementable controllers, has motivated significant research work on the development of a general order reduction procedure, based on combination of the method of weighted residuals and approximate inertial manifolds, which allows deriving low-order ODE approximations that capture the dominant dynamics of particulate processes and can, therefore, serve as an appropriate basis for the design of low-order controllers that can be readily implemented in practice (Chiu and Christofides, 1999). This approach subsequently laid the foundation for the development of a systematic framework for solving a number of important control problems for particulate processes, including the problem of dealing with the highly nonlinear behavior (e.g., owing to complex growth, nucleation, agglomeration and breakage mechanisms, and the Arrhenius dependence of nucleation laws on solute concentration in crystallizers; Chiu and Christofides, 1999), the problem of model uncertainty (Chiu and Christofides, 2000), and the problem of control under actuator constraints (El-Farra et al., 2001).

In the operation of particulate processes, constraints typically arise due to physical limitations on the capacity of control actuators and/or desired restrictions on the process state variables, such as temperature and certain properties of the PSD (e.g., crystal concentration and total particle size), in order to meet some safety or product quality requirements. In current industrial practice, the achievement of optimal performance, subject to input and state constraints, relies to a large extent on the use of model predictive control (MPC) policies which are well known for their ability to handle multi-variable interactions, constraints, and optimization requirements, all in a consistent, systematic manner. Unlike open-loop model-based optimal control policies (where the optimal operating conditions are calculated off-line), in MPC, the control action is computed by solving repeatedly, on-line, a constrained optimization problem at each sampling time. Owing to this, MPC has the ability to suppress the influence of external disturbances and tolerate model inaccuracies (because of the use of feedback) and force the system to follow the optimal trajectory that respects constraints on the operating conditions.

In this work, we focus on the development and application of predictive algorithms for control of PSDs in continuous and batch particulate processes described by PBMs. The control algorithms are designed on the basis of finite-dimensional models that capture the dominant dynamics of the particulate processes and are tailored to address different control objectives for the batch and continuous processes. The controllers utilize real-time measurements of the principal moments of the PSD (such measurements, for example, can be obtained from PSD measurements made by light scattering techniques as in the case of crystallization processes), as well as measurements of the process temperature and of the concentrations of the continuous-phase species. For continuous particulate processes, we consider the control objective of asymptotic stabilization under constraints and develop a hybrid predictive control methodology that employs logic-based switching between MPC and a fall-back bounded controller with a well-defined stability region. The hybrid predictive control strategy provides a safety net for the implementation of MPC algorithms to particulate processes with guaranteed stability regions. The strategy is successfully used to stabilize a continuous crystallizer at an open-loop unstable steady-state. For batch particulate processes, the control objective is to achieve PSD with desired characteristics subject to both control and product quality constraints. An optimization-based predictive control strategy that incorporates these constraints explicitly in the controller design is formulated and applied to a seeded batch crystallizer of potassium sulfate crystals. The strategy is shown to be able to reduce the volume of fines by 13.4% compared to a linear cooling strategy, and to possess a robustness margin with respect to modeling errors.

2. Predictive control of continuous particulate processes

2.1. A continuous crystallizer: modeling and dynamics

Crystallization is a particulate process which is widely used in industry for the production of many products including fertilizers, proteins, and pesticides. The fact that the shape of the crystal-size distribution influences significantly the necessary liquid–solid separation, as well as the properties of the product, implies that crystallization requires

a population balance in order to be accurately described, analyzed, and controlled. Continuous crystallizers typically exhibit highly oscillatory behavior which suggests the use of feedback control to ensure stable operation and attain a crystal-size distribution with desired characteristics. Under the assumptions of isothermal operation, constant volume, mixed suspension, nucleation of crystals of infinitesimal size, and mixed product removal, a dynamic model for a continuous crystallizer can be derived from a population balance for the particle phase and a mass balance for the solute concentration of the following form (Lei et al., 1971; Jerauld et al., 1983):

$$\frac{\partial n}{\partial \bar{t}} = -\frac{\partial (R(\bar{t})n)}{\partial r} - \frac{n}{\tau} + \delta(r-0)Q(\bar{t}),$$
$$\frac{\mathrm{d}c}{\mathrm{d}\bar{t}} = \frac{(c_0-\rho)}{\bar{\varepsilon}\tau} + \frac{(\rho-c)}{\tau} + \frac{(\rho-c)}{\bar{\varepsilon}}\frac{\mathrm{d}\bar{\varepsilon}}{\mathrm{d}\bar{t}}, \quad (1)$$

where $n(r,\bar{t})$ is the density of crystals of radius $r \in [0,\infty)$ at time $\bar{t}$ in the suspension, τ is the residence time, c is the solute concentration in the crystallizer, c_0 is the solute concentration in the feed, and

$$\bar{\varepsilon} = 1 - \int_0^\infty n(r,\bar{t})\frac{4}{3}\pi r^3 \,\mathrm{d}r$$

is the volume of liquid per unit volume of suspension. $R(\bar{t})$ is the growth rate, $\delta(r-0)$ is the standard Dirac function, and $Q(\bar{t})$ is the nucleation rate. The term $\delta(r-0)Q(\bar{t})$ accounts for the production of crystals of infinitesimal (zero) size via nucleation. $R(\bar{t})$ and $Q(\bar{t})$ are assumed to follow McCabe's law and Volmer's nucleation law, respectively:

$$R(\bar{t}) = k_1(c-c_s),$$
$$Q(\bar{t}) = \bar{\varepsilon}k_2 \exp\left[-\frac{k_3}{\left(\frac{c}{c_s}-1\right)^2}\right], \quad (2)$$

where k_1, k_2, and k_3 are constants and c_s is the concentration of solute at saturation.

To study the dynamic behavior of the crystallizer in question, a second-order accurate finite-difference spatial discretization scheme with 1000 discretization points was used to obtain the solution of the system of Eqs. (1)–(2) (simulations of the system using more discretization points led to identical results). The values of the process parameters used in the simulations can be found in Chiu and Christofides (1999).

The solid lines in Fig. 1 show the open-loop profiles of the total crystal concentration and the solute concentration obtained by solving the distributed parameter model of Eqs. (1)–(2). It is clear that the crystallizer exhibits highly oscillatory behavior, which is the result of the interplay between growth and nucleation caused by the relative nonlinearity of the nucleation rate as compared to the growth rate (compare the nonlinear dependence of $Q(\bar{t})$ and $R(\bar{t})$ on c in Eq. (2)). To establish that the dynamics of the crystallizer are

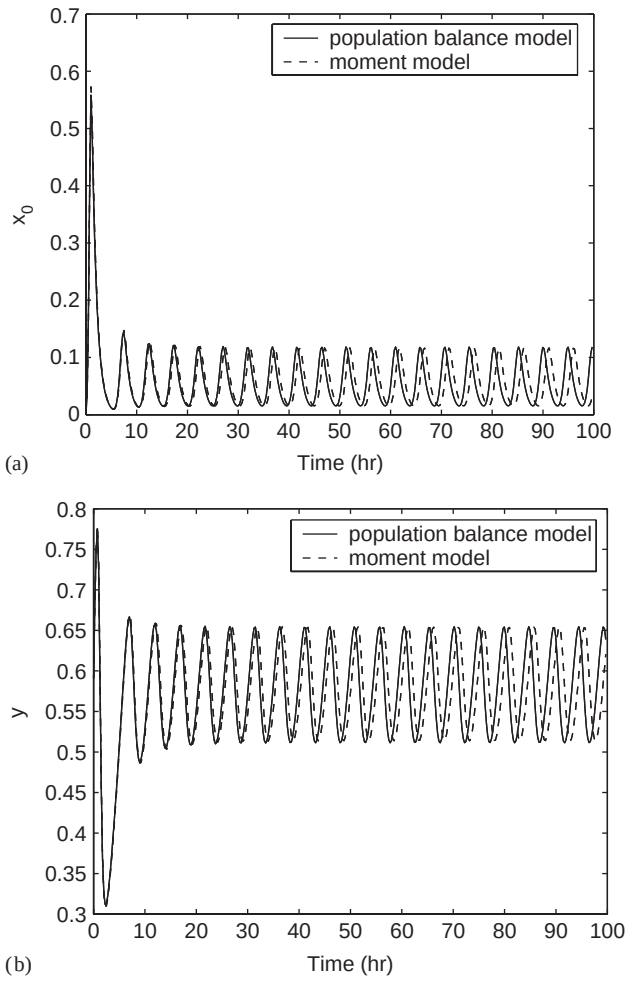

Fig. 1. Comparison of open-loop profiles of (a) crystal concentration and (b) solute concentration obtained from the distributed parameter model and the moments model.

characterized by a small number of degrees of freedom, the method of moments is applied to the system of Eqs. (1)–(2) to derive a reduced-order ODE model. Because the nucleation and growth rates are assumed to be independent of particle size, this allows closure of the moments equations, which results in the reduced-order moments model being an exact replication of the evolution of the dominant modes of the PBM. The differences between the two trajectories in Fig. 1 is only due to numerical errors in the integration of two time-varying systems. It is noted that the method of moments has been extensively used in the past to analyze the dynamics of particulate processes (e.g., Hulburt and Katz, 1964; Pratsinis, 1988).

Defining the jth moment of $n(r,\bar{t})$ as

$$\mu_j = \int_0^\infty r^j n(r,\bar{t})\,\mathrm{d}r, \quad j = 0,\ldots, \quad (3)$$

multiplying the population balance in Eq. (1) by r^j, and integrating over all particle sizes, the following system of

infinite ODEs, which describes the rate of change of the moments of the PSD and the solute concentration, is obtained

$$\begin{aligned}
\frac{d\mu_0}{d\bar{t}} &= -\frac{\mu_0}{\tau} + \left(1 - \frac{4}{3}\pi\mu_3\right) k_2 e^{-k_3/((c/c_s)-1)^2},\\
\frac{d\mu_1}{d\bar{t}} &= -\frac{\mu_1}{\tau} + \nu k_1 (c - c_s)\mu_0,\\
\frac{d\mu_2}{d\bar{t}} &= -\frac{\mu_2}{\tau} + \nu k_1 (c - c_s)\mu_1,\\
\frac{d\mu_3}{d\bar{t}} &= -\frac{\mu_3}{\tau} + \nu k_1 (c - c_s)\mu_2,\\
\frac{d\mu_j}{d\bar{t}} &= -\frac{\mu_j}{\tau} + \nu k_1 (c - c_s)\mu_{j-1}, \quad j = 4, 5, 6, \ldots,\\
\frac{dc}{d\bar{t}} &= \frac{c_0 - c - 4\pi k_1 \tau (c - c_s)\mu_2(\rho - c)}{\tau(1 - (4/3)\pi\mu_3)}.
\end{aligned} \tag{4}$$

On the basis of the system of Eq. (4), it is clear that the moments of order four and higher do not affect those of order three and lower, and moreover, the state of the infinite-dimensional system is bounded when μ_3 and c are bounded, and it converges to a globally exponentially stable equilibrium point when $\lim_{t\to\infty} \mu_3 = c_1$ and $\lim_{t\to\infty} c = c_2$, where c_1, c_2 are constants. This implies that the dominant dynamics of the process of Eq. (1) can be adequately captured by the fifth-order moments model which includes the dynamics of the first four moments and those of the solute concentration. Furthermore, when the following set of dimensionless variables and parameters is introduced:

$$\begin{aligned}
&x_0 = 8\pi\sigma^3\mu_0, \quad x_1 = 8\pi\sigma^2\mu_1, \quad x_2 = 4\pi\sigma\mu_2,\\
&x_3 = \tfrac{4}{3}\pi\mu_3, \ldots,\\
&t = \frac{\bar{t}}{\tau}, \quad \sigma = k_1\tau(c_{0s} - c_s), \quad Da = 8\pi\sigma^3 k_2 \tau,\\
&F = \frac{k_3 c_s^2}{(c_{0s} - c_s)^2}, \quad \alpha = \frac{(\rho - c_s)}{(c_{0s} - c_s)},\\
&y = \frac{(c - c_s)}{(c_{0s} - c_s)}, \quad u = \frac{(c_0 - c_{0s})}{(c_{0s} - c_s)}.
\end{aligned} \tag{5}$$

The resulting moments model takes the form

$$\begin{aligned}
\frac{dx_0}{dt} &= -x_0 + (1 - x_3) Da\ \exp(-F/y^2),\\
\frac{dx_1}{dt} &= -x_1 + y x_0,\\
\frac{dx_2}{dt} &= -x_2 + y x_1,\\
\frac{dx_3}{dt} &= -x_3 + y x_2,\\
\frac{dy}{dt} &= \frac{1 - y - (\alpha - y) y x_2}{1 - x_3} + \frac{u}{1 - x_3},
\end{aligned} \tag{6}$$

where x_i, $i = 0, 1, 2, 3$, are the dimensionless moments of the crystal size distribution, y is the dimensionless concentration of the solute in the crystallizer, and u is the dimensionless concentration of the solute in the feed (the reader may refer to El-Farra et al. (2001) for a detailed derivation of the moments model, and to Christofides (2002) for further results and references in this area).

The stability properties of the fifth-order model of Eq. (6) have been studied thoroughly in Jerauld et al. (1983) (see also Lei et al., 1971), where it is shown that the global phase space of this model has a unique unstable steady-state surrounded by a stable periodic orbit, and that the linearization of the system of Eq. (1) around the unstable steady-state includes two isolated complex conjugate eigenvalues with a positive real part.

2.2. Hybrid predictive controller design

Having obtained a low-order ODE model that captures the dominant dynamics of the continuous crystallizer, we proceed in this section to address the controller synthesis problem on the basis of the low-order model. The control objective is to stabilize the crystallizer at an unstable steady-state (which corresponds to a desired PSD) using constrained control action. MPC is a popular method for handling constraints within an optimal control setting. In MPC, the control action is obtained by solving repeatedly, on-line, a finite-horizon constrained open-loop optimal control problem. When the system is linear, the cost quadratic, and the constraints convex, the MPC optimization problem reduces to a quadratic program for which efficient software exists and, consequently, a number of control-relevant issues have been explored, including issues of closed-loop stability, performance, implementation and constraint satisfaction. The crystallizer, however, exhibits highly nonlinear behavior that must be accounted for when designing the controller. While several nonlinear model predictive control (NMPC) schemes have been proposed in the literature (see Mayne et al. (2000) for a survey of results in this area), the practical implementation of MPC is limited by (1) the computational difficulties of solving a nonlinear (typically nonconvex) optimization problem at each time step, and (2) the difficulty of characterizing, a priori, the set of initial conditions starting from where a given NMPC controller is guaranteed to be feasible and/or stabilize the closed-loop nonlinear system.

To overcome these difficulties, we have recently developed (El-Farra et al., 2004) a hybrid predictive control structure that provides a safety net for the implementation of predictive control algorithms. The central idea is to use a bounded analytical nonlinear controller, with an explicitly characterized stability region, as a fall-back controller, and embed the operation of MPC within its stability region. In the event that the given predictive controller (which can be based on linear or nonlinear models) is unable to stabilize the closed-loop system (e.g., due to failure of the optimization algorithm, poor choice of the initial condition, insufficient horizon length, etc.), supervisory switching from MPC to the bounded controller safeguards closed-loop stability.

In order to proceed with the hybrid predictive controller design, we initially re-write the moments model of Eq. (6) in a more compact form

$$\dot{\tilde{x}}(t) = f(\tilde{x}(t)) + g(\tilde{x}(t))\tilde{u}(t), \quad |\tilde{u}| \leqslant u_{\max}, \tag{7}$$

where $\tilde{x}=[\tilde{x}_0\ \tilde{x}_1\ \tilde{x}_2\ \tilde{x}_3\ \tilde{y}]'$, $\tilde{x}_i = x_i - x_i^s$, $i=0, 1, 2, 3$, $\tilde{y}=y-y^s$, $\tilde{u}=u-u^s$, $u_{\max} \geqslant 0$ denotes the bound on the manipulated input, the superscript at x_i^s refers to the unstable steady-state at which we would like to asymptotically stabilize the system.

In order to provide the necessary background for our main results in Section 2.3, we will briefly review in the remainder of this section the design procedure for, and the stability properties of, both the bounded and model predictive controllers, which constitute the basic components of our hybrid control scheme. For clarity of presentation, we will focus only on the state feedback problem where measurements of $x(t)$ are assumed to be available for all t; the readers may refer to Mhaskar et al. (2004) for results on output feedback hybrid predictive control.

2.2.1. Bounded Lyapunov-based control

Consider the system of Eq. (7), for which a control Lyapunov function (CLF), $V(\tilde{x})$, is available, for more details on the existence and construction of CLFs, see Freeman and Kokotovic (1996). Using the CLF, we construct, using the results in Lin and Sontag (1991), (see also El-Farra and Christofides, 2001, 2003), the following continuous bounded control law:

$$u(\tilde{x}) = -k(\tilde{x})L_g V(\tilde{x}) := b(\tilde{x}), \tag{8}$$

where

$$k(\tilde{x}) = \begin{cases} \dfrac{L_f V(\tilde{x}) + \sqrt{(L_f V(\tilde{x}))^2 + (u_{\max} L_g V(\tilde{x}))^4}}{(L_g V(\tilde{x}))^2 \left[1 + \sqrt{1 + (u_{\max} L_g V(\tilde{x}))^2}\right]}, & L_g V(\tilde{x}) \neq 0, \\ 0, & L_g V(\tilde{x}) = 0, \end{cases} \tag{9}$$

where $L_f V(\tilde{x}) = (\partial V(\tilde{x})/\partial \tilde{x}) f(\tilde{x})$, and $L_g V(\tilde{x}) = (\partial V(\tilde{x})/\partial \tilde{x}) g(\tilde{x})$. An estimate of the constrained stability region of the above controller can be obtained using the level sets of V, i.e.,

$$\Omega = \{\tilde{x} \in \mathbb{R}^n : V(\tilde{x}) \leqslant c^{\max}\}, \tag{10}$$

where $c^{\max} > 0$ is the largest number for which every nonzero element of Ω is fully contained in the set:

$$\Phi = \{\tilde{x} \in \mathbb{R}^n : L_f V(\tilde{x}) < u_{\max} |L_g V(\tilde{x})|\}. \tag{11}$$

2.2.2. Model predictive control

In this section, we consider MPC of the system under control constraints described by Eq. (7). In the literature, several MPC formulations are currently available. For the sake of a concrete illustration, we briefly describe here a standard formulation (we note that any other MPC formulation can be used; see El-Farra et al. (2004) for further details on this issue). For this case, the control action in MPC at state $\tilde{x}$ and time t is conventionally obtained by solving, on-line, a finite horizon optimal control problem of the form

$$\begin{aligned} &P(\tilde{x}, t) : \min\{J(\tilde{x}, t, \tilde{u}(\cdot)) | \tilde{u}(\cdot) \in S\}, \\ &\text{s.t. } \dot{\tilde{x}} = f(\tilde{x}) + g(\tilde{x})\tilde{u}, \end{aligned} \tag{12}$$

where $S = S(t, T)$ is the family of piecewise continuous functions, with period Δ, mapping $[t, t+T]$ into $\mathscr{U} := \{\tilde{u} \in \mathbb{R} : |\tilde{u}| \leqslant u_{\max}\}$ and T is the specified horizon. The constraint in Eq. (12) is a nonlinear model describing the time evolution of the states $\tilde{x}$. A control $\tilde{u}(\cdot)$ in S is characterized by the sequence $\{\tilde{u}[k]\}$ where $\tilde{u}[k] := \tilde{u}(k\Delta)$, and satisfies $\tilde{u}(t) = \tilde{u}[k]$ for all $t \in [k\Delta, (k+1)\Delta)$. The performance index is given by

$$J(\tilde{x}, t, \tilde{u}(\cdot)) = \int_t^{t+T} \left[\|\tilde{x}^u(s; \tilde{x}, t)\|_Q^2 + \|\tilde{u}(s)\|_R^2\right] \mathrm{d}s + F(\tilde{x}(t+T)), \tag{13}$$

where $\|\cdot\|_Q$ refers to the weighted norm, defined by $\|\tilde{x}\|_Q^2 = \tilde{x}'Q\tilde{x}$ for all $\tilde{x} \in \mathbb{R}^n$, Q and R are strictly positive-definite, symmetric matrices and $\tilde{x}^u(s; \tilde{x}, t)$ denotes the solution of Eq. (7), due to control $\tilde{u}$, with initial state $\tilde{x}$ at time t and $F(\cdot)$ denotes the terminal penalty. The minimizing control $\tilde{u}^0(\cdot) \in S$ is then applied to the plant over the interval $t, t+\Delta$ and the procedure is repeated indefinitely. This defines an implicit MPC law

$$M(\tilde{x}) = \text{argmin}(J(\tilde{x}, t, \tilde{u}(\cdot))) = \tilde{u}^0(t; \tilde{x}, t). \tag{14}$$

2.2.3. A hybrid predictive control strategy: switching logic design

In this section, we describe a switching strategy that brings together the MPC and bounded controllers in a way that guarantees asymptotic closed-loop stability and provides a safety net for the implementation of MPC. To this end, consider the constrained nonlinear system of Eq. (7), with any initial condition $\tilde{x}(0) \in \Omega$, where Ω was defined in Eq. (10), under the model predictive controller of Eqs. (12)–(14). Also let $\bar{T} \geqslant 0$ be the earliest time for which either the closed-loop state, under MPC, satisfies

$$L_f V(\tilde{x}(\bar{T})) + L_g V(\tilde{x}(\bar{T})) M(\tilde{x}(\bar{T})) \geqslant 0 \tag{15}$$

or the MPC algorithm fails to prescribe any control move. Then, the switching rule given by

$$\tilde{u}(t) = \begin{cases} M(\tilde{x}(t)), & 0 \leqslant t < \bar{T}, \\ b(\tilde{x}(t)), & t \geqslant \bar{T} \end{cases} \tag{16}$$

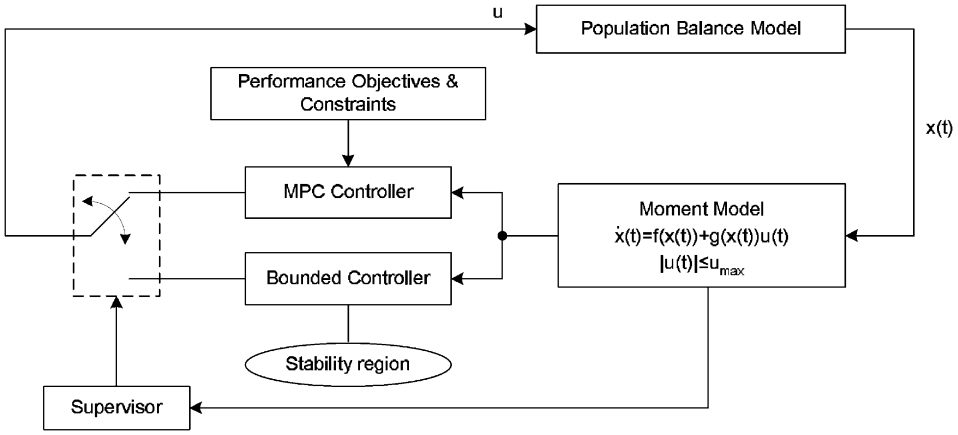

Fig. 2. Closed-loop system under hybrid predictive control.

guarantees that the origin of the switched closed-loop system of Eqs. (7)–(16) is asymptotically stable (see El-Farra et al. (2004) for a detailed proof as well as possible extensions of the switching scheme).

The hybrid predictive control structure consists of the predictive controller, the bounded nonlinear controller with its estimated region of closed-loop stability, and a high-level supervisor that orchestrates the switching between the two controllers. A schematic representation of the hybrid predictive control structure is shown in Fig. 2. The implementation procedure is outlined below:

(1) Consider the population balance model (PBM) of Eqs. (1)–(2) and use the model reduction procedure, based on the method of moments, to derive the finite-dimensional ODE model of Eq. (6) that captures the dominant dynamics of the continuous crystallizer.
(2) Given the constraints on the manipulated input and an appropriate CLF, design the bounded controller, on the basis of the system of Eq. (6), using Eqs. (8)–(9), and compute the stability region using Eqs. (10)–(11).
(3) Given the performance objective and constraints, construct the MPC optimization algorithm, on the basis of the system of Eq. (6), and choose the MPC parameters.
(4) Initialize the closed-loop system under MPC, with the initial condition $x(0)$ belonging to the set Ω.
(5) Monitor the temporal evolution of the closed-loop trajectory of x (by checking Eq. (15) at each time) and denote the earliest time that either Eq. (15) holds or the MPC algorithm prescribes no control move as $\bar{T}$.
(6) If such a $\bar{T}$ exists, discontinue MPC implementation, switch to the bounded controller and implement it for all future times.

2.3. Application to control of PSD in a continuous crystallizer

In this section, we demonstrate the application of the hybrid predictive control strategy to the continuous crystallizer of Eqs. (1)–(2). The control objective is to suppress the oscillatory behavior of the crystallizer and stabilize it at an unstable steady-state that corresponds to a desired PSD by manipulating the inlet solute concentration. To achieve this objective, we assume that the first four moments, as well as the solute concentration, can be measured on-line. Following the proposed methodology, we initially use the moments model of Eq. (6) to design the controllers. The values of the dimensionless model parameters in Eq. (6) are chosen to be: $F = 3.0$, $\alpha = 40.0$ and $Da = 200.0$. The dimensionless solute feed concentration, u, is subject to the constraints: $-1 \leqslant u \leqslant 1$ (which correspond to the following constraint on the inlet solute concentration; $980\,\mathrm{kg/m^3} \leqslant c_0 \leqslant 1000\,\mathrm{kg/m^3}$). The desired steady-state is $x^s = [x_0^s\ x_1^s\ x_2^s\ x_3^s\ y^s]' = [0.065\ 0.040\ 0.024\ 0.015\ 0.612]'$, and $u^s = 0.2$.

To facilitate the design of the bounded controller and construction of the CLF, we initially re-write the moments model of Eq. (6) in deviation variable form—thus translating the steady-state to the origin—to obtain the system of Eq. (7) which we transform into the normal form. To this end, we define the auxiliary output variable, $\bar{y} = h(x) = \tilde{x}_0$, and introduce the invertible coordinate transformation: $[\xi'\ \eta']' = \Pi(x) = [\tilde{x}_0\ f_1(\tilde{x})\ \tilde{x}_1\ \tilde{x}_2\ \tilde{x}_3]'$, where $\xi = [\xi_1\ \xi_2]' = [\tilde{x}_0\ f_1(\tilde{x})]'$, $\bar{y} = \xi_1$, $f_1(\tilde{x}) = -\tilde{x}_0 + (1-\tilde{x}_3)Da\ \exp(-F/\tilde{y}^2)$, and $\eta = [\eta_1\ \eta_2\ \eta_3]' = [\tilde{x}_1\ \tilde{x}_2\ \tilde{x}_3]'$. The state-space description of the system in the transformed coordinates takes the form

$$\begin{aligned} \dot{\xi} &= A\xi + bl(\xi,\eta) + b\alpha(\xi,\eta)u, \\ \dot{\eta} &= \Psi(\eta,\xi), \end{aligned} \tag{17}$$

where $A = \begin{bmatrix} 0 & 1 \\ 0 & 0 \end{bmatrix}$, $b = [0\ 1]'$, $l(\xi,\eta) = L_f^2 h(\Pi^{-1}(\xi,\eta))$ is the second-order Lie derivative of the scalar function, $h(\cdot)$, along the vector field $f(\cdot)$, and $\alpha(\xi,\eta) = L_g L_f h(\Pi^{-1}(\xi,\eta))$ is the mixed Lie derivative. The forms of $f(\cdot)$ and $g(\cdot)$ can be obtained by re-writing the system of Eq. (6) in the form of Eq. (7), and are omitted for brevity.

The partially-linear ξ-subsystem in Eq. (17) is used to design a bounded controller that stabilizes the full interconnected system of Eq. (17) and, consequently, the original system of Eq. (6). For this purpose, a quadratic function of the form, $V_\xi = \xi' P \xi$, is used as a CLF in the controller synthesis formula of Eqs. (8)–(9), where the positive-definite matrix, P, is chosen to satisfy the Riccati matrix equality: $A'P + PA - Pbb'P = -\bar{Q}$ where $\bar{Q}$ is a positive-definite matrix. An estimate of the region of constrained closed-loop stability for the full system is obtained by defining a composite Lyapunov function of the form $V_c = V_\xi + V_\eta$, where $V_\eta = \eta' P_\eta \eta$ and P_η is a positive-definite matrix, and choosing a level set of V_c, Ω_c, for which $\dot{V}_c < 0$ for all x in Ω_c. The two-dimensional projections of the stability region are shown in Fig. 3 for all possible combinations of the system states.

In designing the predictive controller, a linear MPC formulation, with a terminal equality constraint of the form $x(t+T) = 0$, is chosen (based on the linearization of the reduced order model of Eq. (6) around the unstable equilibrium point). The parameters in the objective function of Eq. (13) are taken to be: $Q = qI$, with $q = 1$, $R = rI$, with $r = 1.0$, and $F = 0$. We also choose a horizon length of $T = 0.25$ in implementing the predictive controller. The resulting quadratic program is solved using the MATLAB subroutine QuadProg, and the full nonlinear closed-loop system is integrated using finite-differences.

In the first set of simulation runs, we tested the ability of the predictive controller to stabilize the crystallizer starting from the initial condition, $x(0) = [0.066\ 0.041\ 0.025\ 0.015\ 0.560]'$. The result is shown by the solid lines in Fig. 4(a)–(e) where it is seen that the predictive controller, with a horizon length of $T = 0.25$, is able to stabilize the closed-loop system at the desired equilibrium point. Starting from the initial condition $x(0) = [0.033\ 0.020\ 0.013\ 0.0075\ 0.570]'$, however, the predictive controller yields no feasible solution. If the terminal equality constraint is removed, to make MPC feasible, we see from the dashed lines in Fig. 4(a)–(e) that the resulting control action cannot stabilize the closed-loop system, and leads to a stable limit cycle. Fig. 5 (a) shows the resulting sustained oscillations in the PSD under MPC without terminal constraints. On the other hand, when the hybrid predictive controller is implemented, the supervisor detects initial infeasibility of MPC and implements the bounded controller in the closed loop. As the closed-loop states evolve under the bounded controller and get closer to the desired steady-state, the supervisor finds (at $t = 5.8$) that the MPC becomes feasible and, therefore, implements it for all future times. Note that despite the "jump" in the control action profile as we switch from the bounded controller to MPC at $t = 5.8$, (see the difference between dotted and dash-dotted profiles in Fig. 4(f)), the moments of the PSD in the crystallizer continue to evolve smoothly (dash-dotted lines in Fig. 4(a)–(e)). The supervisor finds that MPC continuous to be feasible and is implemented in closed-loop to stabilize the closed-loop system at the desired steady-state. The dotted lines in Fig. 4(a)–(e) shows the simulation results of the closed-loop system under the bounded controller only. Compared with the simulation results under the bounded controller, the hybrid predictive controller (dash-dotted lines) stabilizes the system much faster, and achieves a better performance, reflected in a lower value of the

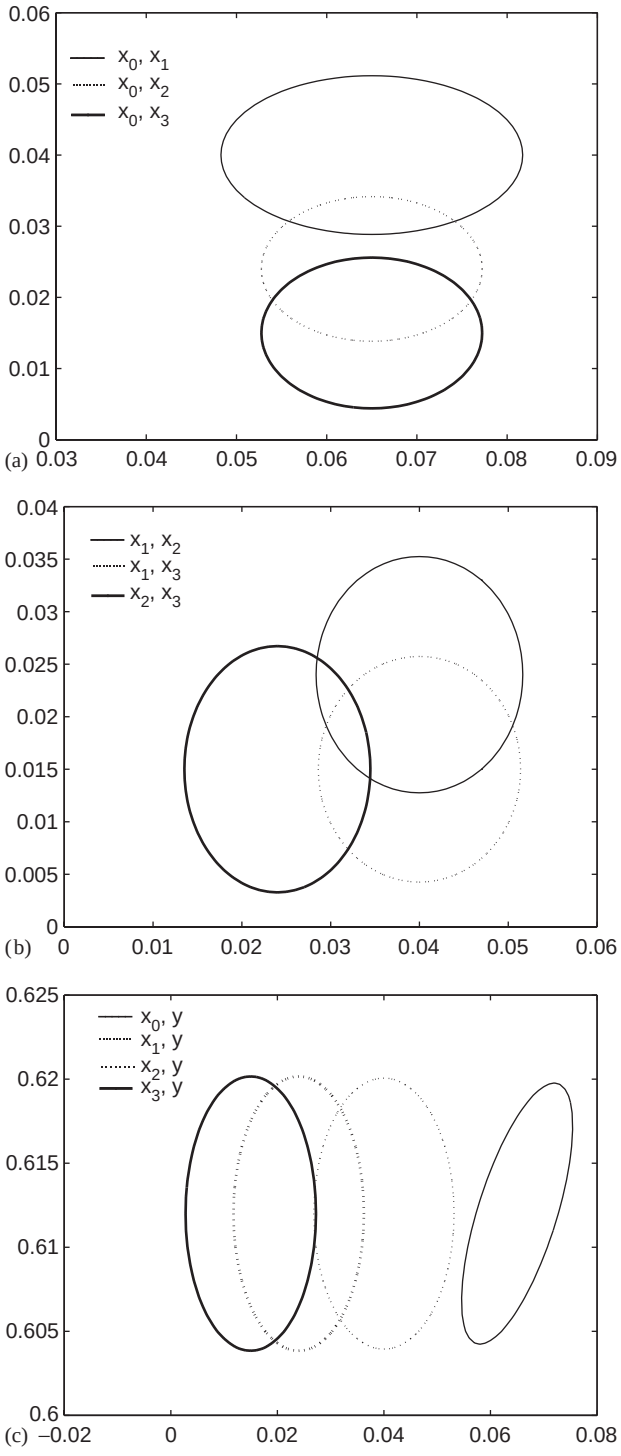

Fig. 3. Two-dimensional projections of the stability region for the 10 distinct combinations of the states of the reduced order system of Eq. (6).

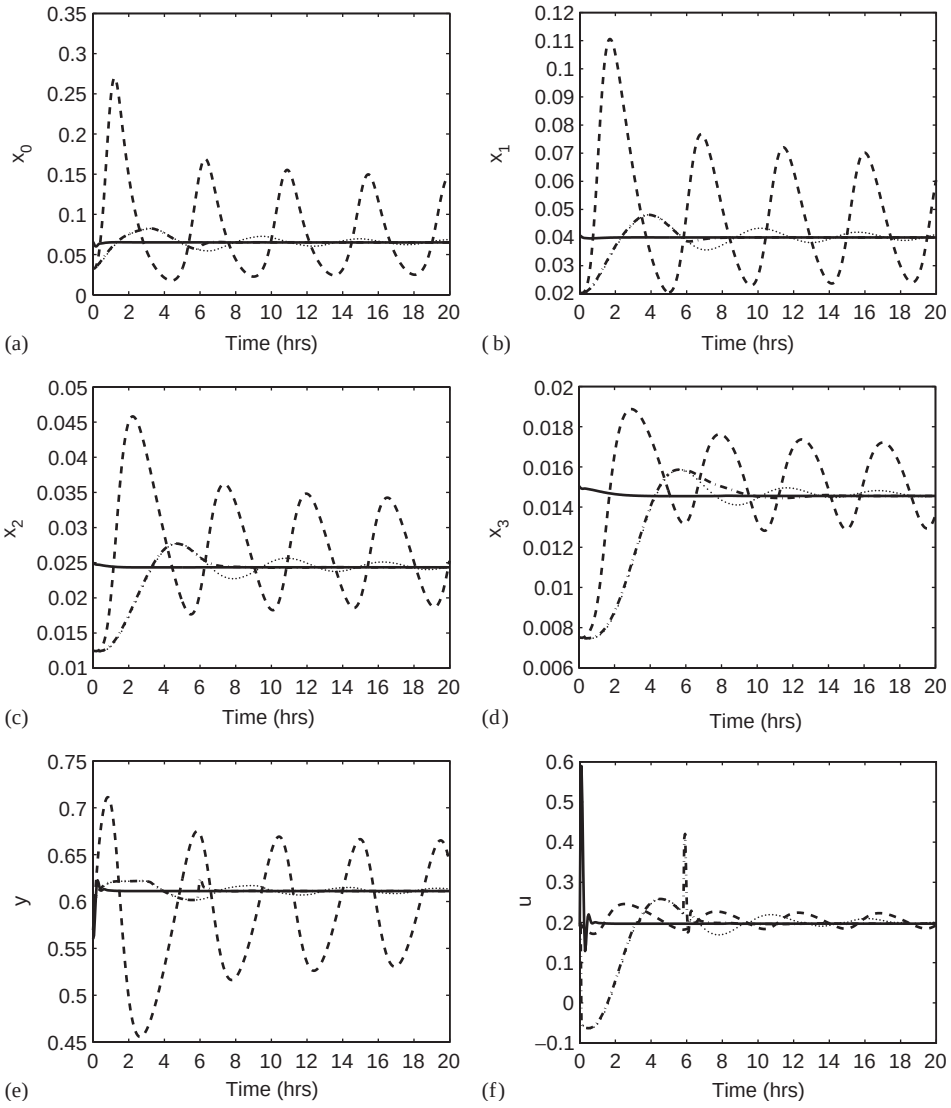

Fig. 4. Continuous crystallizer example: closed-loop profiles of the dimensionless crystallizer moments (a)–(d), the solute concentration in the crystallizer (e) and the manipulated input (f) under MPC with stability constraints (solid lines), under MPC without terminal constraints (dashed lines), under the bounded controller (dotted lines), and using the hybrid predictive controller (dash-dotted lines).

performance index (0.1282 vs. 0.1308). The evolution of PSD under the hybrid predictive controller, shown in Fig. 5(b), illustrates clearly how the hybrid controller stabilizes the PSD at the desired steady state. The manipulated input profiles for the three scenarios are shown in Fig. 4(f).

3. Predictive control of batch particulate processes

Batch crystallization differs from continuous crystallization in that the withdrawal of product for the batch process is made only once at the end of the batch run. It is commonly used in the chemical, pharmaceutical, photographic, and many other industries as manufacturing process to prepare a wide variety of crystalline products. Compared with continuous particulate processes, batch particulate processes have several desirable features (Wey and Karpinski, 2001). For instance, in batch particulate processes, the equipment is relatively simple and flexible, and requires a relatively lower level of maintenance. Batch particulate processes are particularly applicable to chemical systems difficult to process, such as processes with toxic or highly viscous properties. Also, experiments on batch particulate processes can be used to examine a large number of operational variables in a short time. Systems that are difficult to operate continuously may conveniently be investigated in a batch-wise manner with relatively minimum development time and investment. For capacity requirements less than 500 kg/h, batch particulate processes are usually more economically advantageous. Furthermore, if the product requires a relatively narrow PSD, a batch particulate process is clearly a better choice.

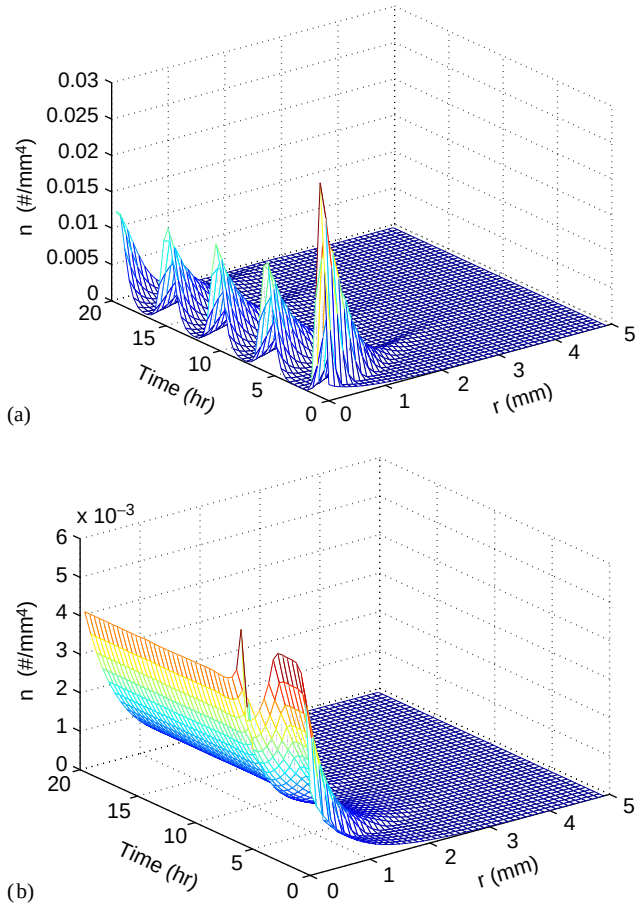

Fig. 5. Closed-loop profiles of the PSD: (a) under MPC without terminal constraints; (b) under the hybrid predictivecontroller.

3.1. A seeded batch crystallizer: modeling and dynamics

As an example, we consider the seeded batch cooling crystallizer studied in Rawlings et al. (1993, 2001), which produces crystals of potassium sulfate. The PBM of this crystallizer, describes the evolution of the crystal size distribution, $n(r,t)$, under the joint effects of nucleation (B is the crystal nucleation rate) and crystal growth (G is the crystal growth rate). The evolution of the solute concentration, C, and reactor temperature, T, are described by two ODEs. The process model has the following form

$$\frac{\partial n(r,t)}{\partial t} + G(t)\frac{\partial n(r,t)}{\partial r} = 0, \quad n(0,t) = \frac{B(t)}{G(t)},$$
$$\frac{\mathrm{d}C}{\mathrm{d}t} = -3\rho k_v G(t)\mu_2(t),$$
$$\frac{\mathrm{d}T}{\mathrm{d}t} = -\frac{UA}{MC_p}(T - T_j) - \frac{\Delta H}{C_p}3\rho k_v G(t)\mu_2(t), \tag{18}$$

where ρ is the density of crystals, k_v is the volumetric shape factor, U is the overall heat-transfer coefficient, A is the total heat-transfer surface area, M is the mass of solvent in the crystallizer, C_p is the heat capacity of the solution, T_j is the jacket temperature, ΔH is the heat of reaction, and

$$\mu_2 = \int_0^\infty r^2 n(r,t)\,\mathrm{d}r$$

is the second moment of the PSD. The nucleation rate, $B(t)$, and the growth rate, $G(t)$, are given by

$$B(t) = k_b \mathrm{e}^{-E_b/RT}\left(\frac{C - C_s(T)}{C_s(T)}\right)^b \mu_3,$$
$$G(t) = k_g \mathrm{e}^{-E_g/RT}\left(\frac{C - C_s(T)}{C_s(T)}\right)^g, \tag{19}$$

where E_b is the nucleation activation energy, E_g is the growth activation energy, b and g are exponents relating nucleation rate and growth rate to supersaturation, C_s is the saturation concentration of the solute, and $\mu_3 = \int_0^\infty r^3 n(r,t)\,\mathrm{d}r$ is the third moment of the PSD. The values of the process parameters are given in Table 1. Eq. (20) below is used to calculate the saturation and metastable concentrations corresponding to the solution temperature T. These two concentrations represent the constraints on the solution concentration, i.e., $C_s \leqslant C \leqslant C_m$ that must hold during the whole batch run. The initial seed distribution of the seeded batch crystallizer is assumed to be a parabolic distribution, from 250 to 300 μm, and the maximum density of initial seed distribution, which is 2/μm g solvent, occurs at 275 μm, i.e., $n(r,0) = 0.0032(300 - r)(r - 250)$, for $250\,\mu\mathrm{m} \leqslant r \leqslant 300\,\mu\mathrm{m}$, and $n(r,0) = 0$, for $r < 250\,\mu\mathrm{m}$ and $r > 300\,\mu\mathrm{m}$.

$$C_s(T) = 6.29 \times 10^{-2} + 2.46 \times 10^{-3}T - 7.14 \times 10^{-6}T^2,$$
$$C_m(T) = 7.76 \times 10^{-2} + 2.46 \times 10^{-3}T - 8.10 \times 10^{-6}T^2. \tag{20}$$

To study the dynamic behavior of the crystallizer, a second-order accurate finite difference scheme with 1500 discretization points is used to obtain the solution of the system of Eq. (18). Fig. 6 shows the evolution of the reactor temperature, T, the solution concentration, C, and the PSD under a linear cooling strategy (where the jacket temperature, T_j, is cooled down linearly from 50 to 30 °C). From Fig. 6(b), it is clear that there is a gap between the crystals formed by nucleation and those growing from the seeds during the whole reaction period. Based on this observation, we developed two moments models to simulate the dynamics of the crystals formed by nucleation and the crystals growing

Table 1
Parameter values for the seeded batch cooling crystallizer of Eqs. (18)–(19)

$b = 1.45$	$g = 1.5$
$k_b = 285.0\,1/(\mathrm{s}\,\mu\mathrm{m}^3)$	$k_g = 1.44 \times 10^8\,\mu\mathrm{m/s}$
$E_b/R = 7517.0\,\mathrm{K}$	$E_g/R = 4859.0\,\mathrm{K}$
$U = 1800\,\mathrm{kJ/m^2\,h\,K}$	$A = 0.25\,\mathrm{m}^2$
$\Delta H = 44.5\,\mathrm{kJ/kg}$	$C_p = 3.8\,\mathrm{kJ/K\,kg}$
$M = 27.0\,\mathrm{kg}$	$\rho = 2.66 \times 10^{-12}\,\mathrm{g}/\mu\mathrm{m}^3$
$k_v = 1.5$	$t_f = 30\,\mathrm{min}$

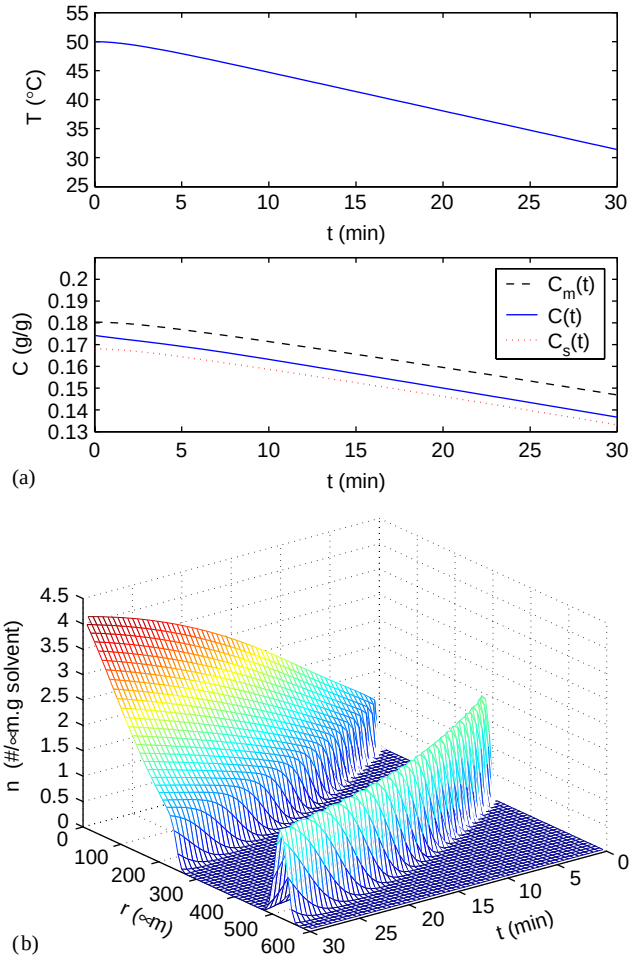

Fig. 6. Simulation results for the linear cooling strategy: (a) reactor temperature and concentration profiles (dashed and dotted lines represent the upper and lower constraints on the concentration, respectively); (b) the evolution of crystal size distribution.

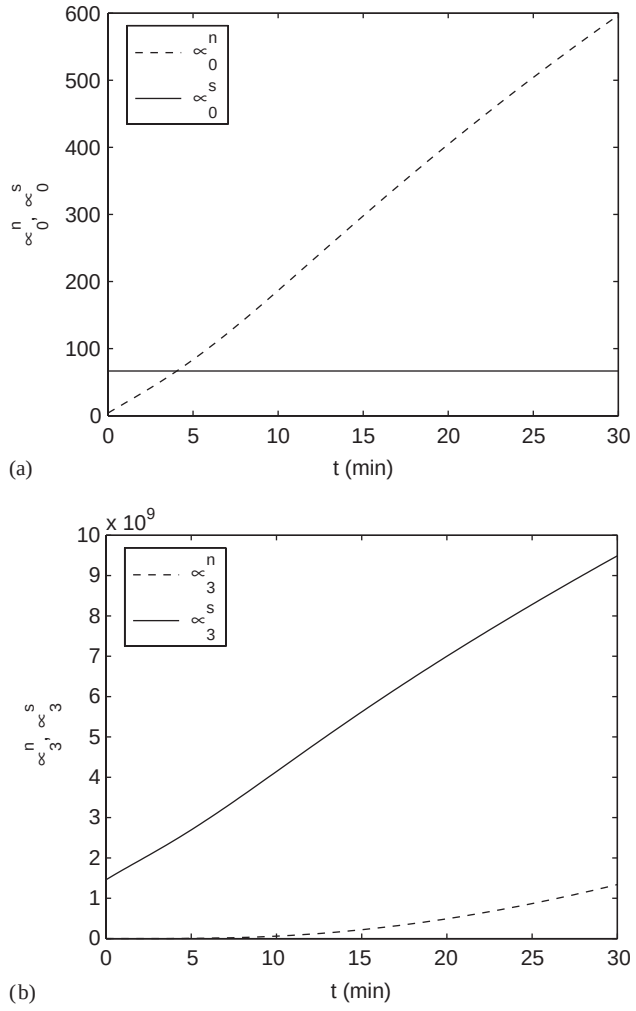

Fig. 7. Simulation results for the linear cooling strategy: the zeroth and third moments of the PSD of the crystals formed by nucleation (dashed lines) and the those growing from the seeds (solid lines).

from the seeds separately. The two models are given by Eqs. (21) and (22), respectively. The mass and energy balances in these two models are described by Eq. (23).

$$\frac{d\mu_0^n}{dt} = B(t),$$
$$\frac{d\mu_i^n}{dt} = iG(t)\mu_{i-1}^n(t), \quad i = 1, 2, 3, \tag{21}$$

$$\mu_0^s = k_4,$$
$$\frac{d\mu_i^s}{dt} = iG(t)\mu_{i-1}^s(t), \quad i = 1, 2, 3, \tag{22}$$

$$\frac{dC}{dt} = -3\rho k_v G(t)\left(\mu_2^n(t) + \mu_2^s(t)\right),$$
$$\frac{dT}{dt} = -\frac{UA}{MC_p}(T - T_j) - \frac{\Delta H}{C_p}3\rho k_v G(t)(\mu_2^n(t) + \mu_2^s(t)), \tag{23}$$

where μ_i^n and μ_i^s $(i = 0, 1, 2, 3)$ are the first four moments of the PSD of the crystals formed by nucleation and the crystals growing from the seeds, respectively, and are defined by

$$\mu_i^n = \int_0^{r_g} r^i n(r, t)\, dr,$$
$$\mu_i^s = \int_{r_g}^{\infty} r^i n(r, t)\, dr, \quad i = 0, 1, 2, 3. \tag{24}$$

The superscript, n, stands for nucleation, and s stands for seed. r_g is the radius at the middle of the gap between two groups of crystals. This characteristic radius is a function of time, and can be determined only from the PBM. Since the model does not consider crystal breakage or agglomeration during the crystallization, μ_0^s, which is the total number of the crystals growing from the seeds, remains constant k_4 during the crystallization period. Fig. 7 shows a comparison between μ_i^n and μ_i^s, $(i = 0, 3)$, based on simulations of the two moments models. The purpose of deriving two moments models instead of one is to facilitate the design of the predictive controller for the PSD of each group of crystals discussed in the next section.

3.2. Predictive controller design: accounting for state and input constraints

Unlike the control of continuous particulate processes, asymptotic stabilization is not an issue in the control of batch processes. More important is the objective of achieving a desired PSD at the end of the batch and satisfying state and control constraints during the whole batch run. Significant previous work has focused on PSD control in the batch crystallizers (e.g., Rawlings et al., 1993; Xie et al., 2001). Mullin and Nyvlt (1971) derived an open-loop optimal control strategy where the objective function involves maximization of the crystal size and the cooling curve is the decision variable. Miller and Rawlings (1994) developed a method for assessing parameter uncertainty and studied its effects on the open-loop optimal control strategy, which maximized the weight mean size of the product. Zhang and Rohani (2003) developed an on-line optimal control methodology for a seeded batch cooling crystallizer to improve the product quality expressed in terms of the mean size and the width of the distribution. Immanuel and Doyle (2003) designed a hierarchical multiobjective strategy to control the PSD in semi-batch emulsion polymerization. In these previous works, most efforts were focused on the open-loop optimal control of the batch crystallizer, i.e., the optimal operating condition was calculated off-line and based on mathematical models. The successful application of such a control strategy relies, to a large extent, on the accuracy of the models.

In this section, we focus on developing a closed-loop predictive control system to minimize the total volume of fines (i.e., small crystals formed by nucleation) in the final product. In the operation of industrial crystallizers, the fines usually cause difficulties in downstream processing equipment (e.g., filtration) and affect both product quality and process economics. Such effects are especially important in a seeded batch crystallizer, since its final products mainly grow from the seeds rather than from the crystal formed by nucleation. Excessive fines may also require a relatively long batch run time to achieve the desired final size of the product. Some experimental studies on fines destruction for batch crystallizers have been reported. Jones et al. (1984) first described the application of fines destruction in batch crystallization of potassium sulfate solutions. Rohani et al. (1990) implemented a feedback control fines dissolution strategy in order to maintain the fines slurry density at some constant value over the batch run. These studies demonstrate the experimental feasibility of dramatically reducing the amount of fines in the final product based on the reactor design.

In this work, a closed-loop predictive control scheme is developed to control the seeded batch cooling crystallizer described by Eq. (18). The control objective is to minimize the volume of fines in the final product, (i.e., the third moment of the crystals formed by nucleation, μ_3^n), by manipulating the jacket temperature, T_j. The principle moments are calculated from the on-line measured PSD, n, which can be obtained by measurement techniques such as the laser light scattering method. The concentration and reactor temperature are also assumed to be measured in real time. In the closed-loop control structure, the PBM, together with the mass and energy balances of Eq. (18), are used to describe the process while the reduced-order model of Eqs. (21)–(22) is used within the MPC for the purpose of prediction. Therefore, the PBM is utilized to simulate the value of the state variables (n, C, T) at $t_i = i\Delta t$, where $i = 1, 2, \ldots, m$, $m = t_f/\Delta t$, and t_f is the length of the crystallization period. Thus, the values of the moments $\left(\mu_j^n(t_i), \mu_j^s(t_i),\ j = 0, 1, 2, 3\right)$ are calculated from the PSD at every t_i, $n(r, t_i)$. The values of $\mu_j^n(t_i)$, $\mu_j^s(t_i)$, $C(t_i)$, $T(t_i)$, and the optimal trajectory of T_j solved at the previous time step, are used as the initial values for the reduced-order model in MPC to solve an optimization problem for a horizon length of $t_f - t_i$. The first step of the solution (T_j) is implemented to generate the value of state variables at the end of next time step, t_{i+1}. This procedure is repeated every Δt until the end of the batch run.

Manipulated input limitations and concentration specifications are incorporated as input and state constraints on the optimization problem, which takes the form

$$\begin{aligned} \min \quad & \mu_3^n(t_f) \\ \text{s.t.} \quad & T_{j,\min} \leqslant T_j \leqslant T_{j,\max}, \\ & C_s \leqslant C \leqslant C_m, \\ & \left\| \frac{\mathrm{d}T_j}{\mathrm{d}t} \right\| \leqslant k_5, \\ & \mu_3^s(t_f) \geqslant V_1, \end{aligned} \tag{25}$$

where μ_3^n, μ_3^s, T_j and C are obtained by solving the moments models of Eqs. (21)–(22). $T_{j,\min}$ and $T_{j,\max}$ are the constraints on the manipulated variable, T_j, and set to 30 and 50 °C in the simulation. C_s and C_m, which can be calculated from Eq. (20), are the constraints on the solution concentration. The constant, k_5, (chosen to be 2 °C/min) is the maximum gradient of the jacket temperature. V_1, chosen as 8.3301×10^9 in the simulations, denotes the lower bound on the total volume of the crystals growing from the seeds. Such constraint on $\mu_3^s(t_f)$ represents a desirable quality of the final product. In the simulation, Δt and t_f are chosen as 30 s and 30 min, respectively. The optimization problem is solved using the steepest descent method, which is a gradient-based optimization method. Considering the high dimensionality of the nonlinear optimization problem, fast convergence is critical to real time implementation of the predictive control policy. Furthermore, the optimization results based on the steepest descent method and SQP were compared, and only a small difference was observed, while the SQP method took a considerably longer time to converge than the steepest descent method.

3.3. Closed-loop simulation results

To illustrate the effect of model accuracy on the ability of the predictive controller to control the crystallizer, we considered two different cases. In the first case, it is assumed

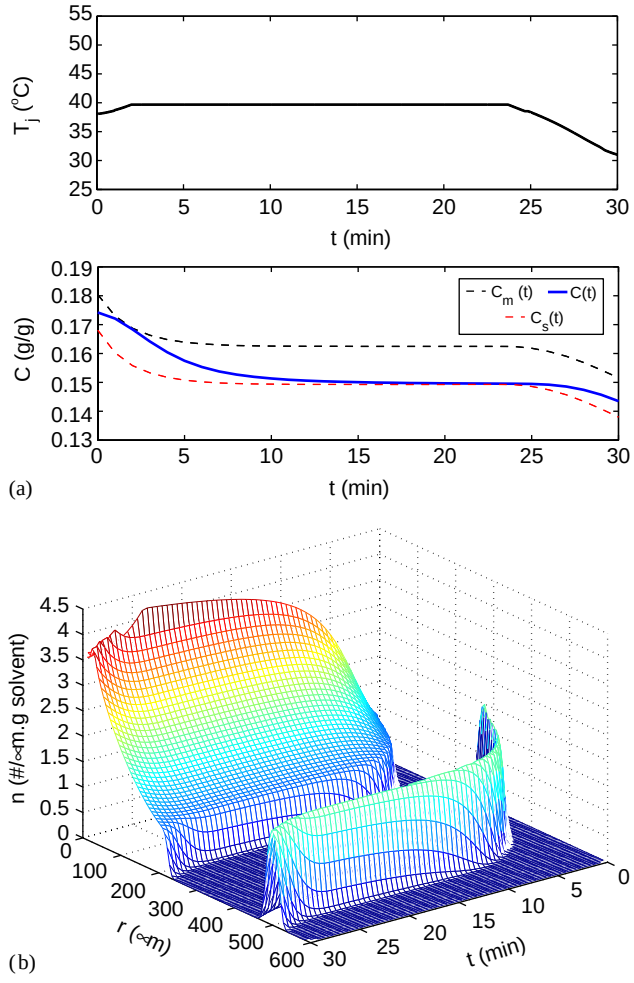

Fig. 8. Closed-loop simulation results for matched models: (a) Jacket temperature and concentration profiles (dashed and dotted lines represent the upper and lower constraints on the concentration, respectively); (b) the evolution of crystal size distribution.

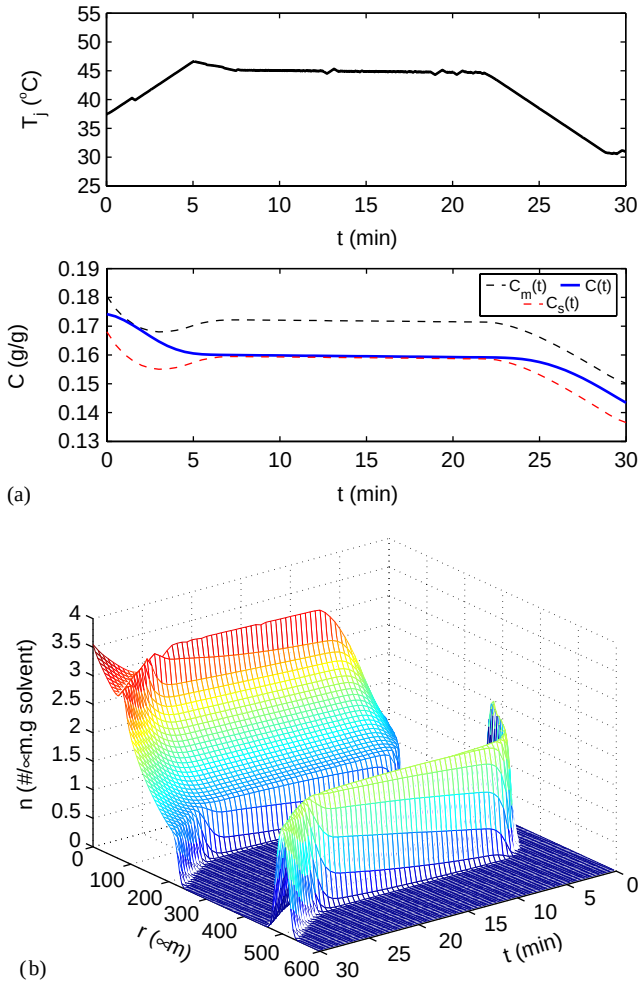

Fig. 9. Closed-loop simulation results for mismatched models: (a) Jacket temperature and concentration profiles (dashed and dotted lines represent the upper and lower constraints on the concentration, respectively); (b) the evolution of crystal size distribution.

that the same model parameters are used in the MPC model (i.e., the moments model) and the process model (i.e., PBM). In another case, a process–model mismatch is introduced by changing the value of the parameter b, which is the exponent relating nucleation rate to supersaturation, from its nominal value of 1.45–1.35 in the moments model used in MPC. The simulation results of these two cases were also compared with the open-loop simulation results obtained under the linear cooling strategy.

Fig. 8 shows the closed-loop simulation results for the case of a perfect process–model match. Fig. 8(a) shows the optimal trajectory of the jacket temperature and solution concentration while Fig. 8(b) shows the evolution of the PSD. Clearly, the constraints on the jacket temperature and concentration are respected during the evolution of the closed-loop profiles. When a process–model mismatch is considered, MPC is unable to satisfy the state and control constraints unless the time step of the closed-loop control system (the hold time in MPC implementation) is lowered from 30 to 15 s, indicating that tighter feedback control is necessary in the case of imperfect model to avoid violation of the constraints. The closed-loop simulation results for the case of a process–model mismatch are shown in Fig. 9. Comparing Figs. 8 and 9, it is clear that the predictive controller produces a different manipulated input trajectory to enforce constraint satisfaction when the model used in MPC design does not perfectly match the process. It is also noticed that the off-line computed optimal trajectory of T_j based on the mismatched model fails to satisfy the constraints on the solute concentration during the batch run. Such results indicate that feedback control is necessary to guarantee that the process operates within the constraints.

Table 2 lists the value of μ_3^n and μ_3^s obtained under four different control strategies: (1) Open-loop with linear cooling, (2) MPC with an objective to maximize μ_3^s/μ_3^n, (3) MPC with the objective of Eq. (25) under a perfect process–model match, and (4) MPC with the objective of Eq. (25) under a process–model mismatch. Fig. 10 compares the final crystal

Table 2
Comparison between the simulation results under four different control strategies

Control strategy	μ_3^n (μm^2/g solvent)	μ_3^s (μm^2/g solvent)
Open-loop with linear cooling	8.9174×10^8	8.3304×10^9
MPC with objective to maximize μ_3^s/μ_3^n	1.7828×10^9	1.0545×10^{10}
MPC with matched moments model	7.7209×10^8	8.3301×10^9
MPC with mismatched moments model	7.8655×10^8	8.3301×10^9

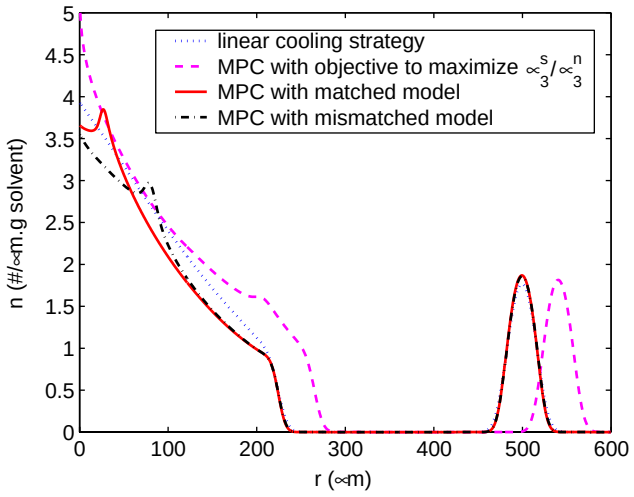

Fig. 10. Comparison of the final crystal size distributions under four different control strategies.

size distribution under these 4 different control strategies. Comparing the results of control strategies (1), (3) and (4), it is clear that MPC can lower the volume of fines (nucleation formed crystals) by 13.4% compared with the linear cooling strategy, while the crystals growing from the seeds in final product still satisfy the product quality requirement. It is also observed that, in the case of process–model mismatch, the predictive control strategy (with a smaller time step) is able to successfully control the system and lower the volume of fines by 11.8% compared with the linear cooling strategy. To demonstrate the effect of the choice of optimization objective in the control strategy on the volume of fines, we carried out simulations with the same control structure, but with a different optimization objective which is to maximize the ratio μ_3^s/μ_3^n. Comparing the results in Table 2, it is clear that, when MPC with this objective is applied, even though the volume of crystals growing from the seeds increases by 26.6% (relative to the linear cooling strategy) which is favorable to product quality, the volume of fines actually increases dramatically by 129.2%. Such large difference on the crystal size distribution of final products can be more clearly seen in Fig. 10. It shows that the control strategy (2) leads to larger crystals formed by both nucleation and grown from seeds compared to the other three control strategies, which allow to produce less crystals formed by nucleation while satisfying the minimum requirement of the volume of the crystals grown from seeds. This result suggests that maximizing the ratio μ_3^s/μ_3^n, while favoring product quality, does so at the expense of a significant increase in the volume of fines which is undesirable. In contrast, the optimization problem of Eq. (25) provides a more meaningful formulation whereby the volume of fines is explicitly minimized, and the product quality is accounted for as a constraint on the optimization problem. This significant difference in the impact on μ_3^s and μ_3^n between the two optimization formulations suggests that the optimization objective should be selected carefully, when attempting to achieve a desired PSD, in order to strike a balance between enhancing product quality and minimizing the difficulties caused by a large volume of fines. Finally, to study the importance of incorporating measurements in the control system, we carried out a simulation of the predictive control system where the values of the state variables at each time step are not updated using measurements from the process, but instead, are updated using the values generated by simulating the moments model with $b=1.35$. In this case, the simulation results (not shown in the manuscript due to space limitation) show that the state constraints are violated at the end of the open-loop simulation run because of the discrepancy between the PBM and the mismatched moments model, and the lack of measurement feedback.

4. Conclusions

In this work, we focused on the development and application of predictive algorithms for control of PSDs in continuous and batch particulate processes described by PBMs. The control algorithms were designed on the basis of finite-dimensional models that capture the dominant dynamics of the particulate processes and were tailored to address different control objectives for the continuous and batch processes. Closed-loop simulations have demonstrated the effectiveness of the proposed control algorithms.

Acknowledgements

Financial support, from the National Science Foundation, CTS-0129571, and a 2001 Office of Naval Research (ONR) Young Investigator Award, is gratefully acknowledged.

References

Chiu, T., Christofides, P.D., 1999. Nonlinear control of particulate processes. A.I.Ch.E. Journal 45, 1279–1297.

Chiu, T., Christofides, P.D., 2000. Robust control of particulate processes using uncertain population balances. A.I.Ch.E. Journal 46, 266–280.

Christofides, P.D., 2002. Model-Based Control of Particulate Processes. Kluwer Academic Publishers, Dordrecht.

Dimitratos, J., Elicabe, G., Georgakis, C., 1994. Control of emulsion polymerization reactors. A.I.Ch.E. Journal 40, 1993–2021.

El-Farra, N.H., Christofides, P.D., 2001. Integrating robustness, optimality and constraints in control of nonlinear processes. Chemical Engineering Science 56, 1841–1868.

El-Farra, N.H., Christofides, P.D., 2003. Bounded robust control of constrained multivariabe nonlinear processes. Chemical Engineering Science 58, 3025–3047.

El-Farra, N.H., Chiu, T., Christofides, P.D., 2001. Analysis and control of particulate processes with input constraints. A.I.Ch.E. Journal 47, 1849–1865.

El-Farra, N.H., Mhaskar, P., Christofides, P.D., 2004. Hybrid predictive control of nonlinear systems: method and applications to chemical processes. International Journal of Robust and Nonlinear Control 14, 199–225.

Freeman, R.A., Kokotovic, P.V., 1996. Robust Nonlinear Control Design: State-Space and Lyapunov Techniques. Birkhauser, Boston.

Friedlander, S.K., 1977. Smoke, Dust, and Haze, Fundamentals of Aerosol Behavior. Wiley, New York.

Gelbard, F., Seinfeld, J.H., 1978. Numerical solution of the dynamic equation for particulate processes. Journal of Computational Physics 28, 357–375.

Hounslow, M.J., 1990. A discretized population balance for continuous systems at steady-state. A.I.Ch.E. Journal 36, 106–116.

Hulburt, H.M., Katz, S., 1964. Some problems in particle technology, a statistical mechanical formulation. Chemical Engineering Science 19, 555–574.

Immanuel, C.D., Doyle III, F.J., 2003. Hierarchical multiobjective strategy for particle-size distribution control. A.I.Ch.E. Journal 49, 2383.

Jerauld, G.R., Vasatis, Y., Doherty, M.F., 1983. Simple conditions for the appearance of sustained oscillations in continuous crystallizers. Chemical Engineering Science 38, 1675–1681.

Jones, A.G., Chianese, A., Mullin, J.W., 1984. Effect of fines destruction on batch cooling crystallization of potassium sulphate solutions. In: Jancic, S.J., de Jong, E.J. (Eds.), Industrial Crystallization, vol. 84, Proceedings of the Ninth Symposium on Industrial Crystallization, pp. 191–195.

Kumar, S., Ramkrishna, D., 1996. On the solution of population balance equations by discretization—II. A moving pivot technique. Chemical Engineering Science 51, 1333–1342.

Lei, S.J., Shinnar, R., Katz, S., 1971. The stability and dynamic behavior of a continuous crystallizer with a fines trap. A.I.Ch.E. Journal 17, 1459–1470.

Lin, Y., Sontag, E.D., 1991. A universal formula for stabilization with bounded controls. Systems & Control Letters 16, 393–397.

Mantzaris, N.V., Daoutidis, P., Srienc, F., 2001. Numerical solution of multi-variable cell population balance models, I. Finite difference methods. Computers & Chemical Engineering 25, 1411.

Mhaskar, P., El-Farra, N., Christofides, P.D., 2004. Hybrid predictive control of process systems. A.I.Ch.E. Journal 50, 1242–1259.

Mayne, D.Q., Rawlings, J.B., Rao, C.V., Scokaert, P.O.M., 2000. Constrained model predictive control, stability and optimality. Automatica 36, 789–814.

Miller, S.M., Rawlings, J.B., 1994. Model identification and control strategies for batch cooling crystallizers. A.I.Ch.E. Journal 40, 1312–1327.

Mullin, J.W., Nyvlt, J., 1971. Programmed cooling of batch crystallizers. Chemical Engineering Science 26, 369–377.

Pladis, P., Kiparissides, C., 1998. A comprehensive model for the calculation of molecular weight-long-chain branching distribution in free-radical polymerizations. Chemical Engineering Science 53, 3315–3333.

Pratsinis, S.E., 1988. Simultaneous nucleation, condensation, and coagulation in aerosol reactors. Journal of Colloid and Interface Science 124, 416–426.

Ramkrishna, D., 1985. The status of population balances. Reviews in Chemical Engineering 3, 49–95.

Randolph, A.D., Larson, M.A., 1988. Theory of Particulate Processes. Second ed. Academic press, San Diego.

Rawlings, J.B., Ray, W.H., 1987. Stability of continuous emulsion polymerization reactors: a detailed model analysis. Chemical Engineering Science 42, 2767–2777.

Rawlings, J.B., Miller, S.M., Witkowski, W.R., 1993. Model identification and control of solution crystallization process. Industrial & Engineering Chemistry Research 32, 1275–1296.

Rawlings, J.B., Slink, C.W., Miller, S.M., 2001. Control of crystallization processes. In: Myerson, A.S. (Ed.), Handbook of Industrial Crystallization, Second ed., pp. 201–230.

Rohani, S., Bourne, J.R., 1990. Self-tuning control of crystal size distribution in a cooling batch crystallizer. Chemical Engineering Science 12, 3457–3466.

Rohani, S., Tavare, N.S., Garside, J., 1990. Control of crystal size distribution in a batch cooling crystallizer. Canadian Journal of Chemical Engineering 68, 260–267.

Semino, D., Ray, W.H., 1995a. Control of systems described by population balance equations—I. Controllability analysis. Chemical Engineering Science 50, 1805–1824.

Semino, D., Ray, W.H., 1995b. Control of systems described by population balance equations—II. Emulsion polymerization with constrained control action. Chemical Engineering Science 50, 1825–1839.

Wey, J.S., Karpinski, P.H., 2001. Batch crystallization. In: Myerson, A.S. (Ed.), Handbook of Industrial Crystallization, Second ed., pp. 231–248.

Xie, W., Rohani, S., Phoenix, A., 2001. Dynamic modeling and operation of a seeded batch cooling crystallizer. Chemical Engineering Communications 187, 229–249.

Zhang, G.P., Rohani, S., 2003. On-line optimal control of a seeded batch cooling crystallizer. Chemical Engineering Science 58, 1887–1896.